

Incompressible strips in dissipative Hall bars as origin of quantized Hall plateaus

Afif Siddiki and Rolf R. Gerhardt

Max-Planck-Institut für Festkörperforschung, Heisenbergstrasse 1, D-70569 Stuttgart, Germany

(Dated: November 18, 2018)

We study the current and charge distribution in a two dimensional electron system, under the conditions of the integer quantized Hall effect, on the basis of a quasi-local transport model, that includes non-linear screening effects on the conductivity via the self-consistently calculated density profile. The existence of “incompressible strips” with integer Landau level filling factor is investigated within a Hartree-type approximation, and non-local effects on the conductivity along those strips are simulated by a suitable averaging procedure. This allows us to calculate the Hall and the longitudinal resistance as continuous functions of the magnetic field B , with plateaus of finite widths and the well-known, exactly quantized values. We emphasize the close relation between these plateaus and the existence of incompressible strips, and we show that for B values within these plateaus the potential variation across the Hall bar is very different from that for B values between adjacent plateaus, in agreement with recent experiments.

PACS numbers: 73.20.-r, 73.50.Jt, 71.70.Di

I. INTRODUCTION

The application of the quantized Hall effect (QHE)¹ as resistance standard, and its importance for modern metrology, relies on the extremely high reproducibility (better than 10^{-8}) of certain quantized resistance values.² This extreme reproducibility points to an universal origin, which is independent on special material or sample properties. The purpose of the present paper is to propose and evaluate a quasi-local transport model that allows us to calculate, first, the potential and current distribution in a two-dimensional electron system (2D ES) under the conditions of the QHE, and, second, the longitudinal and the Hall resistance, $R_L(B)$ and $R_H(B)$, in the plateau regimes of the QHE and in between. Whereas the resistance values between the QH plateaus will depend on details of the used conductivity model, the exactly quantized plateau values result from the existence of sufficiently wide “incompressible strips” along which the local conductivity vanishes, since occupied and unoccupied states are separated by an energy gap (Landau quantization). Localization assumptions,³ which played an important role in early approaches to the QHE, are not included in our model. Our model is motivated by a recent experimental investigation of the Hall-potential in a narrow Hall bar,⁴ and a critical reexamination of a subsequent model calculation.⁵

Experimental information about the actual current and potential distribution in a Hall bar under QHE conditions has been obtained recently by Ahlswede and coworkers^{4,6,7} with a scanning force microscope⁸. The data were interpreted in terms of “incompressible strips” with constant electron density (corresponding to the filling of an integer number of Landau levels),^{9,10,11,12} which are expected to develop in an inhomogeneous 2D ES as a consequence of its strongly non-linear low-temperature screening properties¹³ in a strong perpendicular magnetic field. If the filling factor in the center of the sample was slightly larger than an integer, the Hall potential was

found to drop completely across two strips, while being constant elsewhere. With decreasing B , the strips moved towards the sample edges, just as one expects for the incompressible strips in a sample, in which the electron density decreases gradually from a maximum in the center towards the edges. If the center filling factor was slightly below an integer, a gradual potential variation was observed, either linear or a non-linear, without clear indication for incompressible strips.⁴

This interpretation was supported by subsequent theoretical work of Güven and Gerhardt (GG)⁵, who extended the self-consistent Thomas-Fermi-Poisson approximation (TFPA)^{11,12,13} for the calculation of electron density profile and electrostatic potential to a non-equilibrium situation with a position-dependent electrochemical potential, determined by the presence of an applied dissipative current through the sample. Electrochemical potential and current density was calculated from a local version of Ohm’s law, with a local model for the conductivity tensor, determined by the position-dependent electron density. The feed-back of the current distribution on electron density and the measurable potential profile⁴ was included by the assumption of local equilibrium in the stationary non-equilibrium situation.

In agreement with the experiment⁴, the calculation⁵ shows a linear variation of the Hall potential across the sample if there are no incompressible strips, e.g. for sufficiently high temperature or if the magnetic field is so strong, that the local filling factor is everywhere in the sample less than two (spin-degeneracy is assumed and interactions which might lead to the fractional quantized Hall effect are neglected). Also for center filling factors slightly larger than 2 or 4 the calculation confirms the experiment, showing that the potential drops across broad incompressible strips and is constant elsewhere. However, due to the use of the TFPA, GG⁵ obtain incompressible strips whenever the center filling factor is larger than 2,^{9,10,11,12} and due to the strictly local conductivity model these dominate the current and potential distribu-

tion, and lead to vanishing longitudinal resistance. Thus, the model assumptions of Ref.5 lead to serious disagreement with important aspects of the experiment.

The purpose of the present paper is to improve on the model of GG⁵ so that, first, qualitative agreement between the calculated and the measured potential distribution is achieved for all filling factor regimes, and, second, reasonable results for $R_l(B)$ and $R_H(B)$ are obtained. Following the lines suggested by GG⁵, we investigate in Sec. II the conditions for the existence of incompressible strips, using a Hartree approximation. In Sec. III we reexamine and weaken the strictly local conductivity model, and show that a simple spatial-averaging procedure of the local conductivities can simulate corrections expected from a Hartree calculation for the equilibrium state and from a non-local transport calculation. Transport results based on the self-consistent Born approximation will be presented and discussed in Sec. IV. In the present work we will restrict our consideration on the linear response regime, so that heating effects, which might destroy incompressible strips in the presence of high currents,⁵ can be neglected.

II. EXISTENCE OF INCOMPRESSIBLE STRIPS

A. Electrostatic self-consistency

Following Ref.5, we consider a 2D ES in the plane $z = 0$, with translation invariance in the y direction and an electron density $n_{\text{el}}(x)$ confined to the interval $-d < x < d$. The confinement potential $V_{bg}(x)$ is determined by fixed background charges and boundary conditions on metallic gates. The mutual Coulomb interactions between the electrons are treated in a Hartree-type approximation, i.e., are replaced by a potential energy term $V_H(x)$ which is determined via Poisson's equation by the electron density. Exchange and correlation effects are neglected, and spin degeneracy is assumed. Thus, the electrons move in an effective potential

$$V(x) = V_{bg}(x) + V_H(x), \quad (1)$$

$$V_H(x) = \frac{2e^2}{\bar{\kappa}} \int_{-d}^d dx' K(x, x') n_{\text{el}}(x'), \quad (2)$$

where $-e$ is the charge of an electron, $\bar{\kappa}$ an average background dielectric constant, and the kernel $K(x, x')$ solves Poisson's equation under the given boundary conditions. Kernel and background potential for the frequently used model,^{9,10,11,12} that assumes all charges and gates to be confined to the plane $z = 0$, are taken from Ref.5,

$$K(x, x') = \ln \left| \frac{\sqrt{(d^2 - x^2)(d^2 - x'^2)} + d^2 - x'x}{(x - x')d} \right|, \quad (3)$$

$$V_{bg}(x) = -E_{bg}^0 \sqrt{1 - (x/d)^2}, \quad E_{bg}^0 = 2\pi e^2 n_0 d / \bar{\kappa}, \quad (4)$$

where n_0 is the homogeneous density of positive background charges in the Hall bar. Other meaningful and tractable boundary conditions are also possible.¹³

To perform explicit calculations, one needs a prescription to calculate the electron density for given effective potential $V(x)$, which then together with Eqs. (1) and (2) completes the electrostatic self-consistency. The self-consistent TFPA^{5,11,12,13} takes this prescription from the Thomas-Fermi approximation (TFA)

$$n_{\text{el}}(x) = \int dE D(E) f(E + V(x) - \mu^*), \quad (5)$$

with $D(E)$ the density of states (DOS), $f(E) = 1/[\exp(E/k_B T) + 1]$ the Fermi function, μ^* the electrochemical potential (being constant in the equilibrium state), k_B the Boltzmann constant, and T the temperature.

B. Hartree approximation

A less restrictive approximation would be to insert $V(x)$ into Schrödinger's equation,

$$\left[\frac{1}{2m} \left(\mathbf{p} + \frac{e}{c} \mathbf{A} \right) + V(x) \right] \Phi_\lambda(\mathbf{r}) = E_\lambda \Phi_\lambda(\mathbf{r}), \quad (6)$$

with $\mathbf{A}(\mathbf{r})$ a vector potential describing the magnetic field $\mathbf{B} = (0, 0, B) = \nabla \times \mathbf{A}$, and to calculate the density from the eigen-energies E_λ and -functions $\Phi_\lambda(\mathbf{r})$,

$$n_{\text{el}}(\mathbf{r}) = \sum_\lambda |\Phi_\lambda(\mathbf{r})|^2 f(E_\lambda - \mu^*). \quad (7)$$

Exploiting the symmetry of our system, we may use the Landau gauge, $\mathbf{A}(\mathbf{r}) = (0, Bx, 0)$, and factorize the wavefunctions, $\Phi_\lambda(\mathbf{r}) = L_y^{-1/2} \exp(iky) \phi_{n,X}(x)$, with L_y a normalization length, $X = -l^2 k$ a center coordinate, $l = \sqrt{\hbar/m\omega_c}$ the magnetic length, and $\omega_c = eB/(mc)$ the cyclotron frequency. The Schrödinger equation then reduces to

$$\left[-\frac{\hbar^2}{2m} \frac{d^2}{dx^2} + \frac{m}{2} \omega_c^2 (x - X)^2 + V(x) \right] \phi_{n,X}(x) = E_n(X) \phi_{n,X}(x), \quad (8)$$

and the electron density becomes

$$n_{\text{el}}(x) = \frac{g_s}{2\pi l^2} \sum_n \int dX f(E_n(X) - \mu^*) |\phi_{n,X}(x)|^2, \quad (9)$$

where $g_s = 2$ takes the spin degeneracy into account and the sum over X has been replaced by an integral, $L_y^{-1} \sum_X \Rightarrow (2\pi l^2)^{-1} \int dX$.

C. Thomas-Fermi Approximation (TFA)

If the potential $V(x)$ varies slowly on the scale of the magnetic length l , its effect on the lowest Landau levels

(LLs) can be treated perturbatively, with the lowest order result

$$E_n(X) \approx E_n + V(X), \quad E_n = \hbar\omega_c(n + 1/2). \quad (10)$$

On the length scale relevant for the variation of $V(x)$, the extent of the Landau wavefunctions may be neglected, $|\phi_{n,X}(x)|^2 \approx \delta(x - X)$. Then the Hartree result for the electron density, Eq. (9), reduces to the TFA, Eq. (5), with the Landau DOS

$$D(E) = \frac{1}{\pi l^2} \sum_{n=0}^{\infty} \delta(E - E_n). \quad (11)$$

To evaluate the self-consistent TFPA we follow Ref.5. First we fix the sample width $2d$ and the density of positive background charges n_0 , and thereby according to Eq. (4) the background potential $V_{bg}(x)$ and the relevant screening parameter $\alpha_{sc} \equiv \pi a_0/d$, with $a_0 = \bar{\kappa} \hbar^2 / (2me^2)$ the screening length ($2a_0 = 9.79$ nm for GaAs). Next we choose the actual width $2b$ of the density profile at $T = 0$ and $B = 0$, and solve for $|x| \leq b$ the linear integral equation⁵

$$V(x) - V_{bg}(x) = \frac{1}{\alpha_{sc}} \int_{-b}^b \frac{dx'}{d} K(x, x') [\mu_0^* - V(x')], \quad (12)$$

[with $\mu_0^* = V(-b) = V(b)$] to which the self-consistent TFPA reduces in this limit. From the corresponding density profile $n_{el}(x; B = 0, T = 0) = D_0[\mu_0^* - V(x)]$, with $D_0 = m/(\pi \hbar^2)$ the DOS of the 2D ES at $B = 0$, we calculate $V(x)$ for $|x| \leq d$, the average density $\bar{n}_{el} = \int_{-d}^d dx n_{el}(x; B = 0, T = 0) / 2d$ with the corresponding Fermi energy $E_F = \bar{n}_{el} / D_0$, and, for later reference, the Fermi energy $E_F^0 = n_{el}(0; B = 0, T = 0) / D_0$ corresponding to the electron density at the center.

In the following we will consider only symmetric density profiles and take b , or equivalently the depletion length $d - b$, as a free parameter, that fixes the density profile and the electro-chemical potential μ_0^* at $B = 0$ (where the temperature dependence is weak). In real samples μ_0^* may be determined by an electron exchange between the 2D ES and its surrounding, which may be possible at high but not at low temperatures. A restriction that fixes μ_0^* will also determine the value of b .

Next, we fix the value of the magnetic field and start with a high temperature to calculate the electron density from Eqs. (5) and (11) self-consistently with Eq. (2), using the previously calculated potential $V(x)$ as initial value. Finally we lower T stepwise until the required low temperature is reached, and iterate (using a Newton-Raphson approach) at each temperature until convergence is achieved.

The solid lines of Fig. 1 show results for $d = 1.5 \mu\text{m}$ and $n_0 = 4 \cdot 10^{11} \text{cm}^{-2}$ (which implies $E_{bg}^0 = 4.38 \text{eV}$) obtained for 501 equidistant mesh points, $-d = x_0 < x_n < x_N = d$ ($N = 500$). The density profile was fixed by choosing $b/d = 0.9$, which yields $\bar{n}_{el} = 2.9 \cdot 10^{11} \text{cm}^{-2}$ and $n_{el}(0; B = 0, T = 0) = 3.58 \cdot 10^{11} \text{cm}^{-2}$, and thus, with

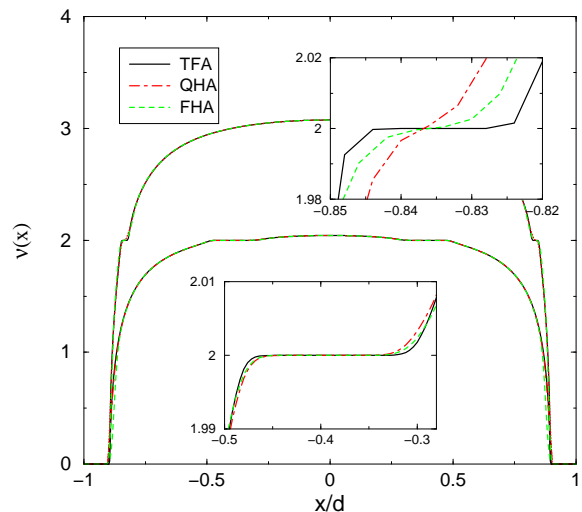


FIG. 1: Electron density profiles for two values of the magnetic field ($\hbar\omega_c/E_F^0 = 0.94$ and 0.65) and different approximations: Thomas-Fermi (solid lines), Hartree (dashed), and quasi-Hartree (dash-dotted). The insets show the enlarged plateau regions for both cases. $\alpha = 0.01$, $k_B T/E_F^0 = 0.0124$. Kinks in the upper inset indicate mesh points.

$D_0 = 2.8 \cdot 10^{10} \text{meV}^{-1} \text{cm}^{-2}$ for AlGa, $E_F = 10.37 \text{meV}$ and $E_F^0 = 12.75 \text{meV}$. We prefer to use E_F^0 (rather than E_{bg}^0) as an reference energy, since it has the same order of magnitude as the cyclotron energies of interest. For finite B we define an effective center filling factor $\nu_0 = 2\pi l^2 n_{el}(x=0; B=0, T=0) = 2E_F^0/\hbar\omega_c$.

The result obtained for the TFPA (solid lines in Fig. 1) shows the expected well developed incompressible strips with constant electron density at local filling factor $\nu(x) = 2$. For the larger B value we obtain wide density plateaus at $0.32 \leq |x|/d \leq 0.46$, in each of which we find at 36 x_n values, with high accuracy, $\nu(x_n) = 2$. For the lower B value the incompressible strips are much narrower, however we obtain the high precision values $\nu(x_n) = 2$ still at five neighboring x_n values. Typical results of the TFPA are summarized in Fig. 2, which shows, as a gray scale plot, the filling factor profile for varying magnetic field, with horizontal lines corresponding to a fixed B value. At sufficiently large B field, the local filling factor $\nu(x)$ is everywhere in the Hall bar less than 2, and the 2D ES is completely compressible. At somewhat lower B ($\hbar\omega_c/E_F^0 \approx 1$) the center of the sample becomes incompressible with local filling factor $\nu(x) = 2$, while $\nu(x)$ gradually decreases outside the incompressible center and falls off to zero in the depletion regions at the sample edges. With further decreasing B , the filling factor in the center increases and incompressible strips with $\nu(x) = 2$ move towards the sample edges and become narrower. At sufficiently low B values, incompressible strips with local filling factor $\nu(x) = 4$ occur, first in the center, and then move towards the edges. They then coexist with incompressible strips of $\nu(x) = 2$, which exist near the edges and are narrow, but, within the TFPA,

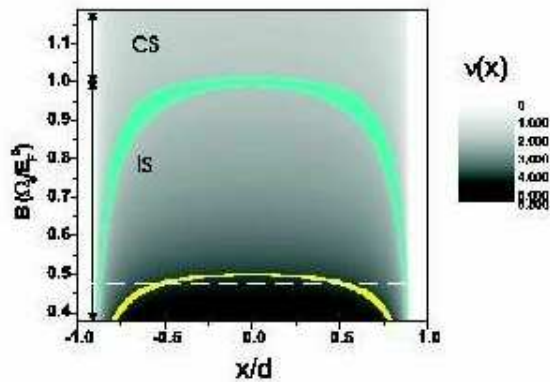


FIG. 2: (color online) Gray scale plot of filling factor versus position x and magnetic field B , calculated within the TFPA. The regions of incompressible strips with $\nu(x) = 2$ and $\nu(x) = 4$ are indicated. For sufficiently large B ($\Omega_c \equiv \hbar\omega_c > E_F^0$) the system is compressible (indicated by “CS”), while for the lower B values included in the figure it always contains incompressible strips (“IS”). The dashed horizontal line refers to Fig. 5 below; $\alpha = 0.01$, $k_B T/E_F^0 = 0.0124$.

still have a finite width. For low enough temperature, this type of behavior continues at still lower values of B , where further incompressible strips with successively higher filling factors evolve from the center and move towards the edges, coexisting with the edge-near incompressible strips of lower local filling factors.

D. “Quasi-Hartree” Approximation

The dashed lines in Fig. 1 are calculated in the Hartree approximation. We started again at $B = 0$, $T = 0$ and inserted in each of the following iteration steps the previously calculated potential $V(x)$ into the eigenvalue problem of Eq. (8), took each mesh point x_n as center coordinate X and diagonalized the problem in the space spanned by the eight lowest-energy unperturbed Landau-Hermite functions

$$\phi_{n,X}^0(x) = \frac{\exp(-[x-X]^2/2l^2)}{\sqrt{2^n n! \sqrt{\pi} l}} H_n([x-X]/l), \quad (13)$$

where $H_n(\xi)$ is the n -th order Hermite polynomial. The resulting energy eigenvalues and -functions were used to calculate the electron density according to Eq. (9). The overall appearance of the Hartree results for the density profiles and also the wide plateaus for the higher B value (see lower inset of Fig. 1) are in good agreement with those of the TFA. The narrow plateaus, obtained in the TFA for the lower B value, are now however smeared out. As is clearly seen in the upper inset of Fig. 1, the Hartree result for the filling factor $\nu(x)$ crosses the value 2 with a finite slope.

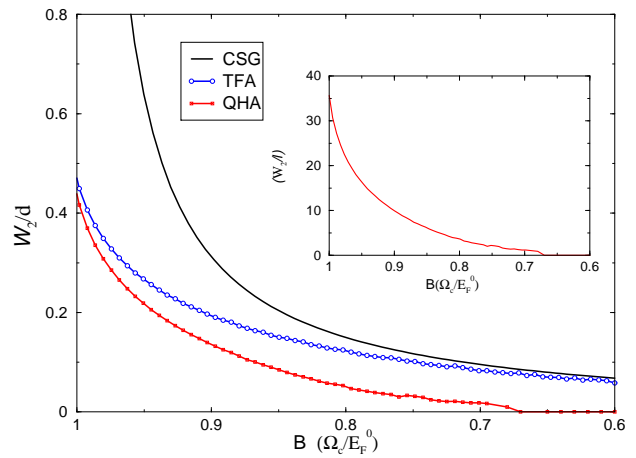


FIG. 3: Magnetic-field dependence of the width of the $\nu = 2$ incompressible strips, for three different approximations: the analytical result of Ref.9 (CSG), the TFPA (TFA), and the quasi-Hartree approximation (QHA). Note the inverted B scale. Inset: ratio of the incompressible strip width to the magnetic length in QHA.

The essential qualitative difference between the Hartree approximation and the TFA is the neglect of the extent of the wavefunctions in the latter. So we interpret the smearing-out of narrow incompressible strips in the Hartree approximation as being due to the finite width of the wave functions. To check this idea, we consider a “quasi-Hartree” approximation (QHA) in which, instead of solving the problem of Eq. (8), we replace the wavefunctions by the eigenfunctions (13) of the unconfined Landau problem and take the energy eigenvalues from Eq. (10). The latter would be correct in the sense of a lowest order perturbation approximation with respect to the effective confining potential $V(x)$, if $V(x)$ would be a linear function of position over the extent of the unperturbed wavefunction $\phi_{n,X}^0(x)$. The numerical effort with this QHA is much less than that required for the full Hartree approximation, since no numerical calculation of energy eigenvalues and -functions is necessary. Density profiles calculated within this QHA are also shown in Fig. 1 as dotted lines. It is seen that the results are very similar to those of the full Hartree calculation, in particular also the results for the smearing-out of the incompressible strips. Apparently the smearing effect of the QHA is even stronger than that of the full Hartree approximation. This is understandable, since the Hartree wavefunctions are asymmetrically squeezed in space regions of a rapid variation of $V(x)$, and therefore have a smaller spatial extent than the unperturbed Landau wavefunctions.

In Fig. 3 we compare the widths of incompressible strips with $\nu(x) = 2$ for several approximations. The line labeled CSG is the analytical half-plane result of Chklovskii *et al.*⁹, $\bar{a}_{\nu_{ic}} = 16\sqrt{a_0 d_0 / \pi} \sqrt{\nu_{ic} / [\nu_0^2 - \nu_{ic}^2]}$, with $d_0 \sim 150$ nm a depletion length, ν_{ic} ($= 2$) the filling factor of the incompressible strip, and $\nu_0 = 2E_F^0 / \hbar\omega_c$ the

effective filling factor.¹¹ This result agrees well with the corresponding self-consistent result of Ref. 11 and for sufficiently low B values (note the inverted B scale in Fig. 3) also with our present TFPA result for samples of finite width. For small B values, the width decreases proportional to B , and remains finite throughout the figure.

The result calculated from our QHA is also included in Fig. 3. As for the TFPA, we have determined the width of the incompressible strips by a simple extrapolation, using three points next to a plateau to determine a plateau edge. For wide plateaus (large B values), the QHA width is only slightly smaller than that calculated within the TFA. However, with decreasing B the QHA width decreases faster and goes to zero at a relatively large magnetic field ($\hbar\omega_c/E_F^0 \approx 0.7$), far before the incompressible strips with $\nu(x) = 4$ develop in the center of the sample.

These results require a modification of Fig. 2. Within the Hartree-type approximation, the width of the incompressible strip with filling factor 2 shrinks more rapidly with decreasing B and vanishes at $\hbar\omega_c/E_F^0 \approx 0.7$. Between this B value and the value $\hbar\omega_c/E_F^0 \approx 0.5$ no incompressible strips exist in the sample. At still lower B values there is a B -interval in which only incompressible strips with local filling factor 4 can exist. This modification required by the QHA is indicated in Fig. 7 below.

In view of the following it may be interesting to note that the essential effects of the Hartree-type approximations can be simulated in a very simple way. If we first perform a calculation within the TFPA and then take a spatial average, e.g., $\bar{\nu}(x) = (2\lambda)^{-1} \int_{-\lambda}^{\lambda} dx' \nu(x+x')$, of the filling factor profile $\nu(x)$, we will smear-out incompressible strips of a width less than 2λ , while incompressible strips with a width larger than 2λ will survive. With λ of the order of the magnetic length, we will obtain filling factor profiles $\bar{\nu}(x)$ very similar to those obtained in the Hartree approximation.

III. INCOMPRESSIBLE STRIPS AND DISTRIBUTION OF DISSIPATIVE CURRENT

A. The local conductivity model

We now describe the effect of an applied current on our Hall bar system, following again the approach of Ref. 5. In the presence of a dissipative current I , the electrochemical potential $\mu^*(\mathbf{r})$ will become position dependent, and its gradient $\mathbf{E} = \nabla\mu^*/e$ will drive the current density $\mathbf{j}(\mathbf{r})$. We assume the linear local relation (Ohm's law)

$$\mathbf{j}(x) = \hat{\sigma}(x) \mathbf{E}(x), \quad \hat{\sigma}(x) = \hat{\sigma}(n_{\text{el}}(x)), \quad (14)$$

with a position-dependent conductivity tensor $\hat{\sigma}(x)$, which has the same form as for a homogeneous sample, however with the homogeneous density replaced by the local electron density $n_{\text{el}}(x)$. Due to the translation invariance in the y direction, which is indicated in Eq. (14),

and the equation of continuity, the components j_x and E_y of current density and electric field, respectively, must be constant,⁵

$$j_x(x) \equiv 0, \quad E_y(x) \equiv E_y^0. \quad (15)$$

For the other components one finds

$$j_y(x) = \frac{1}{\rho_l(x)} E_y^0, \quad E_x(x) = \frac{\rho_H(x)}{\rho_l(x)} E_y^0, \quad (16)$$

in terms of the longitudinal component $\rho_l = \rho_{xx} = \rho_{yy}$ and the Hall component $\rho_H = \rho_{xy} = -\rho_{yx}$ of the resistivity tensor $\hat{\rho} = \hat{\sigma}^{-1}$. For a given applied current $I = \int_{-d}^d dx j_y(x)$ one obtains for the constant electric field component along the Hall bar

$$E_y^0 = I \left[\int_{-d}^d dx \frac{1}{\rho_l(x)} \right]^{-1}, \quad (17)$$

and for the Hall voltage across the sample

$$V_H = \int_{-d}^d dx E_x(x) = E_y^0 \int_{-d}^d dx \frac{\rho_H(x)}{\rho_l(x)}. \quad (18)$$

With the usual normalization of the resistances to a square-shaped conductor, this yields for the Hall and the longitudinal resistance

$$R_H = \frac{V_H}{I}, \quad R_l = \frac{2dE_y^0}{I}. \quad (19)$$

Here we see the essence of the local model. Any reasonable model for the conductivity of a high-mobility 2D ES at zero temperature will give simple results for the conductivity components at even-integer filling factors (where no elastic scattering is possible):

$$\begin{aligned} \sigma_l(\nu=2k) &= \rho_l(\nu=2k) = 0, & (20) \\ \sigma_H(\nu=2k) &= \frac{1}{\rho_H(\nu=2k)} = \frac{e^2}{h} 2k. & (21) \end{aligned}$$

Thus, if an incompressible strip of finite width exists in the sample, the integral in Eq. (17) diverges and E_y^0 and, therefore, the longitudinal resistance R_l is zero. At low temperatures, $k_B T \ll \hbar\omega_c$, $\rho_l(\nu=2k)$ and, therefore, R_l will be exponentially small and relevant contributions to the integral come only from the incompressible regions.

The integral in Eq. (18) has the same type of singularity. If only incompressible strips with the same value $\nu(x) = 2k$ of the local filling factor exist, this singular integral is just the $2k$ -fold of the integral in Eq. (17), so that we get the quantized result $R_H = h/(2ke^2)$. At zero temperature one can evaluate the singular integrals by first introducing a cutoff, e.g. by replacing $\rho_l(x)$ with $\rho_l^\epsilon(x) = \max[\epsilon, \rho_l(x)]$, then calculating the integrals, and finally removing the cutoff ($\epsilon \rightarrow 0$). This yields exact quantization of the Hall resistance, and the corresponding calculation at very low temperatures yields exponentially small corrections. If incompressible strips of finite

widths with different values of $\nu(x)$ exist, e.g. due to a manipulation of the background potential, other values for the Hall resistance may be possible. But, as we have learned from the Hartree-type approximations in the previous section, such a situation will not occur in our simple translation-invariant Hall bar geometry. From these arguments we expect in the resistance-versus-B curves plateau regions of finite widths, where the resistances have the well known quantized values.

These considerations are quite general and do not depend on details of the conductivity model. On the other hand, if we want to calculate the resistances between the plateau regions, we need to specify a conductivity model, and the results will depend on details of this model. We will present such detailed results in Sec. IV below.

B. Limitations of the local model

In Sec. II we have shown that, within a Hartree-type approximation, incompressible strips of a width smaller than the extent of typical wavefunctions cannot exist. As a consequence, incompressible strips with a given filling factor $2k$ do exist only in a finite interval of magnetic fields. For lower B values, the $\nu(x)$ profile crosses the value $2k = \nu(\tilde{x}_{2k})$ with finite slope at some point $x = \tilde{x}_{2k}$. At zero temperature, the integrals in Eqs. (17) and (18) become singular since $\rho_l(\tilde{x}_{2k}) = 0$. Whether the singularity is integrable or not depends on the filling-factor-dependence of the longitudinal conductivity, $\sigma_l(\nu)$. For the SCBA model, to be considered below, it is integrable, for the Gaussian model considered by GG it is not. But should we worry about such sophisticated questions depending on details of the conductivity model? We think we should not, for the following reasons.

All quantities that are related by Eq. (14), the current density, the conductivity and the gradient of the electrochemical potential, represent local values of physical variables, which are defined by macroscopic statistical arguments. In principle, they have to be calculated as average values over sufficiently small subsystems, which nevertheless should contain many electrons. We can not expect that the local relation (14) still holds on a length scale of the order of the mean distance between the constituents of our 2D ES, or, equivalently, of the order of the Fermi wavelength λ_F . On such a length scale one should consider a non-local version of Ohm's law instead. This would, however, make things much more complicated, and we will not enter such problems.

In order to simulate qualitatively the expected effects of a non-local treatment, we start as before with a local model for the conductivity tensor, take the spatial average over a length scale of the order of λ_F , e.g. with $\lambda = \lambda_F/2$ as

$$\hat{\sigma}(x) = \frac{1}{2\lambda} \int_{-\lambda}^{\lambda} d\xi \hat{\sigma}(x + \xi), \quad (22)$$

and use still the local version (14) of Ohm's law, but now

with the averaged conductivity tensor (22). As a consequence, the resistivity components occurring in Sec. III A have to be calculated by tensor inversion of $\hat{\sigma}(x)$.

This simple simulation of non-local effects has several appealing aspects. First, if $\sigma_l(x)$ vanishes at an isolated position $x = \tilde{x}_{2k}$, the averaged $\bar{\sigma}_l(x) > 0$ will be positive in the neighborhood of \tilde{x}_{2k} , and the integrals in Eqs. (17) and (18) will not be singular. Intervals of vanishing $\bar{\sigma}_l(x)$ will exist only, if we start before averaging with sufficiently wide incompressible strips (wider than 2λ). Finally, for high-mobility systems, the Hall conductivity is given to a very good approximation by the free-electron value $\sigma_H(x) = (e^2/h)\nu(x)$. Thus, the averaged Hall conductivity $\bar{\sigma}_H(x)$ will be given by the averaged filling factor profile $\bar{\nu}(x)$. As mentioned at the end of Sec. II, this averaged profile will agree qualitatively with the Hartree profile, if we start with the TFPA profile $\nu(x)$ and average over $\lambda \sim l$ (l the magnetic length). Since for the large magnetic fields of our interest $l \lesssim \lambda_F$, there is actually no need to perform the time consuming Hartree calculation, if we finally want to calculate the averaged conductivity tensor (22).

To summarize, our approximation scheme that simulates both, the effect of finite width of the wavefunctions in the thermal equilibrium calculation, and non-local effects on the transport, is as follows. We calculate the density profile $\nu(x)$ within the self-consistent TFPA, and with this the conductivity tensor $\hat{\sigma}(\nu(x))$. Then we perform the averaging of Eq. (22) and follow the calculations described in Sec. III A. In contrast to Ref. 5 we restrict our calculations here to the linear response regime and do not investigate the feedback of the applied current on the electron density and the electrostatic potential, that is mediated in principle by the position-dependent electrochemical potential $\mu^*(\mathbf{r})$ in the presence of a dissipative current.

C. Self-consistent Born approximation

In principle we could use the conductivity models of Ref. 5 in order to calculate explicit examples. We prefer, however, to take the transport coefficients from the self-consistent Born approximation (SCBA),^{14,15,16} which allows for consistent models of longitudinal and Hall conductivities, and for the consideration of anisotropic scattering by randomly distributed finite-range impurity potentials. We assume that the relevant scatterers are charged donors distributed randomly in a plane parallel to that of the 2D ES, with an areal density n_I , and we approximate the impurity potentials by Gaussian potentials

$$v(\mathbf{r}) = \frac{V_0}{\pi R^2} \exp\left(-\frac{r^2}{R^2}\right), \quad (23)$$

with a range R of the order of the the spacing between 2D ES and doping layer.

An important aspect of the SCBA is that, similar to the “lowest order cumulant approximation” used in Ref. 5, it allows us to treat the transport coefficients and the collision broadening of the LLs in a consistent manner. The relevant SCBA results for the transport coefficients and the collision broadening of a homogeneous 2D ES are summarized in the appendix. Consistency with the transport coefficients requires that we replace in the self-consistent TFPA calculations the δ -functions of the Landau DOS (11) by the semi-elliptic spectral functions (A.5). In addition to the range R , the impurity strength V_0 and concentration n_I determine these quantities via the relaxation time τ_0 defined by the energy $\hbar/\tau_0 = n_I V_0^2 m/\hbar^2$. In strong magnetic fields, this energy combines with the cyclotron energy to

$$\Gamma^2 = 4n_I V_0^2 / (2\pi l^2) = (2/\pi) \hbar\omega_c \hbar/\tau_0, \quad (24)$$

where Γ is the width of the LLs in the limit of zero-range scattering potentials ($R \rightarrow 0$). We find it convenient to characterize the impurity strength by the dimensionless ratio $\gamma = \Gamma/\hbar\omega_c$ at the strong magnetic field $B = 10$ T and define (for GaAs), therefore, the strength parameter

$$\gamma_I = [(2n_I V_0^2 m/\pi\hbar^2)/(17.3 \text{ meV})]^{1/2}. \quad (25)$$

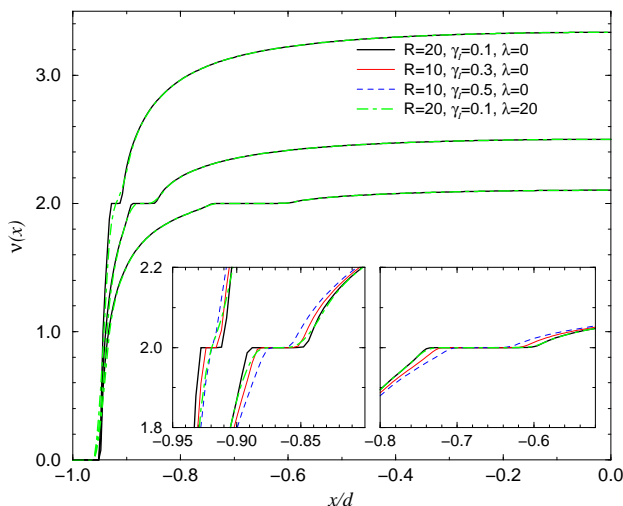


FIG. 4: Filling factor $\nu(x) \approx h\sigma_H(x)/e^2$ versus position in the left half of a symmetric high-mobility ($R = 20$ nm, $\gamma_I = 0.1$) Hall bar of width $d = 1.5 \mu\text{m}$, for three values of the magnetic field, $\hbar\omega_c/E_F^0 = 0.6, 0.8,$ and 0.95 , and without ($\lambda = 0$, solid black lines) and with ($\lambda = 20$ nm, long-dashed green lines) averaging according to Eq. (22). The insets show the plateau regions (incompressible strips) enlarged and include in addition two results for larger collision broadening but no averaging ($\lambda = 0$). Other specifications in the text.

Figure. 4 shows the effect of collision broadening on the density profile at strong magnetic fields. The sample parameters are $d = 1.5 \mu\text{m}$, $n_0 = 4 \cdot 10^{11} \text{cm}^{-2}$ and $b/d = 0.952$, resulting in $\bar{n}_{\text{el}} = 3.37 \cdot 10^{11} \text{cm}^{-2}$ and $E_F = 12.02 \text{ meV}$, $E_F^0 = 13.51 \text{ meV}$. Data are shown for

$t = k_B T/E_F^0 = 0.01$, three values of the magnetic field ($\hbar\omega_c/E_F^0 = 0.6, 0.8,$ and 0.95 , corresponding to central filling factors $\nu(0) = 3.33, 2.5,$ and 2.1 , respectively), and for three sets of the impurity parameters R and γ_I . It is seen from Fig. 4 and Table I that, for sufficiently small collision broadening (small γ_I and, eventually, large R), incompressible strips still may exist, that their width decreases, however, with increasing broadening of the LLs. Table I shows, for several sets of impurity parameters, the relative widths γ_n of the lowest LLs and the zero field mobilities. Data for the second set ($R = 10$ nm, $\gamma_I = 0.1$) are not included in Fig. 4, since they could not be distinguished from the traces for the first, high-mobility set. From the insets of Fig. 4 it is evident that incompressible strips can only survive, if the gap between the broadened LLs remains broad enough. A large collision broadening (low-mobility set No. 4) has a similar effect as a spatial averaging (long-dashed lines in Fig. 4) and may smear out the incompressible strips.

No.	R [nm]	γ_I	γ_0	γ_1	γ_2	$\mu_{B=0}$
1	20	0.1	0.07	0.06	0.05	747.5
2	10	0.1	0.11	0.08	0.07	75.1
3	10	0.3	0.34	0.24	0.21	8.34
4	10	0.5	0.56	0.40	0.35	3.00

TABLE I: Relative width $\gamma_n = \Gamma_n/\hbar\omega_c$ of the Landau levels $n = 0, 1, 2$ at $\hbar\omega_c/E_F^0 = 0.6$, and mobility $\mu_{B=0}$ at $B = 0$, $T = 0$ in units of m^2/Vs , for four sets of model parameters R, γ_I .

IV. RESULTS AND DISCUSSION

A. Effect of spatial averaging

The effect of spatial averaging, introduced to simulate non-local effects on the scale of the Fermi wavelength, is illustrated in Fig. 5. It shows, for a magnetic field value corresponding to a central filling factor $\nu(0) = 4.18$, the filling factor profile calculated with the SCBA broadened DOS, together with the conductivity profiles, Fig. 5(a). Here we have assumed a short-range potential (leading to the rather low mobility $\mu_{B=0} = 6.4 \text{ m}^2/\text{Vs}$), in order to obtain a noticeable deviation of the $\sigma_H(x)$ trace from that for the filling factor $\nu(x)$. Clear incompressible strips with the quantized values for $\sigma_H(x)$ and vanishing $\sigma_L(x)$ are visible where $\nu(x)$ assumes the integer values 4 and 2. The effect of spatial averaging on the conductivities is demonstrated in (b) and (c). The wide (~ 90 nm) plateau defined by $\nu(x) = 4$ shrinks due to the averaging (to ~ 50 nm) but clearly survives, as is shown in Fig. 5(b) for $\sigma_L(x)$, and hold similarly for the plateau of $\sigma_H(x)$. On the other hand, the plateau behavior near the narrow (~ 25 nm) strip defined by $\nu(x) = 2$ is completely smeared out, and $\sigma_L(x)$ does no longer vanish in this region, Fig. 5(c). This has, of course, drastic consequences for the current distribution, which is dom-

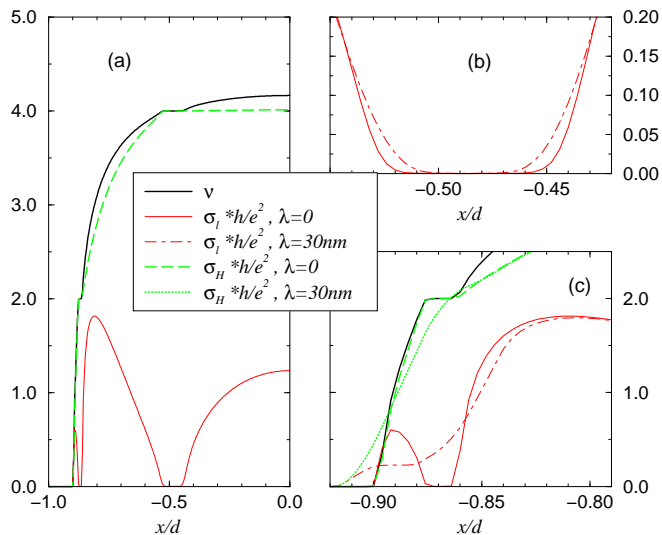


FIG. 5: (a) Filling factor and conductivity profiles for the left half of a symmetric sample with $d = 1.5 \mu\text{m}$, $n_0 = 4 \cdot 10^{11} \text{cm}^{-2}$, $b = 0.9d$, calculated within the SCBA, for $R = 0.1 \text{nm}$ and $\gamma_I = 0.1$, $\hbar\omega_c/E_F^0 = 0.48$, and $k_B T/E_F^0 = 0.01$. (b) and (c) repeat the data of (a) (solid lines) near the incompressible strips with filling factors $\nu(x) = 4$ and $\nu(x) = 2$, respectively. The dash-dotted lines demonstrate the effect of spatial averaging, according to Eq. (22), with $\lambda = 30 \text{nm}$.

inated by the strips with vanishing $\sigma_l(x)$, i.e., vanishing $\rho_l(x)$, see Eq. (16). Without averaging a finite fraction of the total current would flow through the incompressible strips with $\nu(x) = 2$ (on both sides of the sample). With the averaged conductivity tensor, the total current must flow through the incompressible strips with $\nu(x) = 4$ (assuming that there $\sigma_l(x) = 0$ holds exactly).

The mechanism illustrated in Fig. 5 is, of course, also effective at other values of the magnetic field. At larger B with $\nu(0) \gtrsim 2$, broad incompressible strips with $\nu(x) = 2$ will exist near the center of the Hall bar, and the spatially averaged conductivities will show clear plateau behavior. With decreasing B , the incompressible strips move from the center towards the sample edges and shrink. If the strip width becomes of the order of 2λ or smaller, the averaging according to Eq. (22) will destroy the plateau behavior of the conductivities and $\bar{\sigma}_l(x)$ will no longer vanish near the strips. Then the current density still may have a (finite) maximum near the strips with $\nu(x) = 2$, but a finite amount of current will spread over the bulk of the sample, and the global resistances will no longer have the quantized values $R_H = h/2e^2$ and $R_l = 0$.

Figure 6 shows typical results for the dependences of the global resistances on magnetic field and averaging length, as calculated from Eq. (19). At high magnetic fields, $\hbar\omega_c > E_F^0$, we have everywhere in the sample $\nu(x) < 2$, and no incompressible strips exist. The filling factor and consequently the conductivities and the current density vary slowly across the sample. Thus, the spatial averaging has little effect and, within the accu-

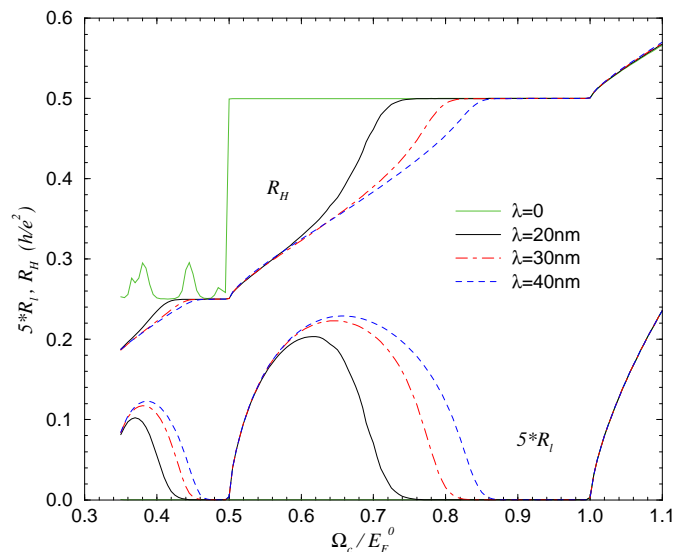


FIG. 6: Calculated Hall and longitudinal resistances versus scaled magnetic field $\hbar\omega_c/E_F^0$, for different values of the averaging length λ . The sample parameters are $d = 1.5 \mu\text{m}$, $n_0 = 4 \cdot 10^{11} \text{cm}^{-2}$, $b = 0.952d$, $R = 10 \text{nm}$ and $\gamma_I = 0.1$, and $k_B T/E_F^0 = 0.01$.

racy of the figure, the results with and without averaging agree. For slightly lower magnetic fields, $\hbar\omega_c \lesssim E_F^0$, broad incompressible strips exist near the center of the sample and, for all the considered averaging lengths λ , strips of finite width with $\sigma_l(x) = 0$ and $\sigma_H(x) = 2e^2/h$ survive. As a consequence, the resistances are quantized, independently on the width of these strips.

For still lower B values the situation becomes more complicated. Within the TFPA, incompressible strips exist for all these B values. Without spatial averaging, $\sigma_l(x)$ vanishes on these strips and, as a consequence, $R_l = 0$, and, for $\hbar\omega_c/E_F^0 > 0.5$, $R_H = h/2e^2$, as shown by the traces for $\lambda = 0$. For $\hbar\omega_c/E_F^0 < 0.5$ there are two types of incompressible strips, with $\sigma_H(x) = 2e^2/h$ or $4e^2/h$, and, without averaging, both contribute according to their widths to R_H , while still $R_l = 0$. The fluctuations in the R_H curve for $\lambda = 0$ result from our TFPA calculation on a finite mesh ($N = 500$), which yields discontinuous changes of the widths of the incompressible strips with changing B . This unsatisfactory picture, obtained for $\lambda = 0$, results from the model calculation of Ref. 5.

The introduction of the spatial averaging improves this situation dramatically and leads to qualitatively correct results. With decreasing B the incompressible strips with $\nu(x) = 2$ become narrower. As the width becomes smaller than 2λ , $\bar{\sigma}_l(x)$ no longer vanishes, the integrals in Eqs. (17) and (18) and thus R_l become finite. This happens at higher B values if λ is larger, and the resistances near the low-magnetic-field edge of the quantum Hall plateau depend strongly on λ . While $\bar{\sigma}_l(x)$ may have a sharp minimum near the strips with $\nu(x) = 2$ if the width of these strips is only slightly smaller than 2λ ,

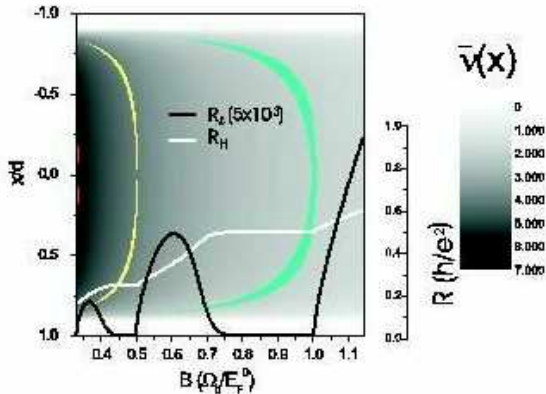


FIG. 7: Calculated Hall resistance (light solid line) and (scaled) longitudinal resistance (black solid line) versus magnetic field, measured in units of $\hbar\omega_c/E_F^0$. The underlying gray scale plot shows the averaged filling factor profile, as in Fig. 2. The crescent-like areas indicate the regions of incompressible strips with local filling factors 2 (right) and 4 (left).

this minimum, and also the corresponding maximum of the current density, will smoothen out as the width of the strips becomes much smaller than 2λ . Then the total resistances will become nearly independent of λ , as is seen in Fig. 6 for $0.5 < \hbar\omega_c/E_F^0 \lesssim 0.6$. For $\hbar\omega_c/E_F^0 \lesssim 0.5$, $\bar{\sigma}_l(x)$ vanishes only within the incompressible strips with $\nu(x) = 4$, but not in strips with $\nu(x) = 2$. As a consequence, we obtain again the exactly quantized results for R_H and R_L .

To visualize the intimate connection between the existence of incompressible strips of finite width [now with constant $\bar{\sigma}_l(x) \approx e^2\bar{\nu}(x)/h$], we show in Fig. 7 a gray scale plot of the spatially averaged filling factor profile for a relevant interval of magnetic fields, together with the resulting resistances.

B. Effect of temperature and collision broadening

The spatial averaging procedure is essential to obtain quantum Hall (QH) plateaus of finite width for the $R_L(B)$ and the $R_H(B)$ curves and to obtain the correct quantized values for $R_H(B)$ on the plateaus corresponding to filling factors larger than two. The width of the calculated QH plateaus does, however, not only depend on the averaging length λ , but also on the temperature and on the broadening of the LLs due to the impurity scattering, since both affect the width of the incompressible strips. The effect of collision broadening on the width of incompressible strips has been indicated in Fig. 4. The temperature effect has been investigated in Ref. 11, where it was shown that, in the absence of collision broadening, i.e., on the basis of the bare Landau DOS (11), the incompressible strips have a finite width at zero temperature. At finite, increasing temperatures, the width

shrinks (while the value of the filling factor remains exactly constant within the remaining strip) until at a sufficiently high temperature ($k_B T \lesssim \hbar\omega_c/25$ in Ref. 11) the width collapses to zero. A similar result is expected in the presence of collision broadening. In particular we expect that, within the self-consistent TFPA based on the SCBA DOS, the existence of an energy gap between two adjacent broadened LLs will always lead to an incompressible strip, provided the temperature is low enough. The necessary temperature will be the lower, the narrower the gap is. But we will not discuss these questions in further details.

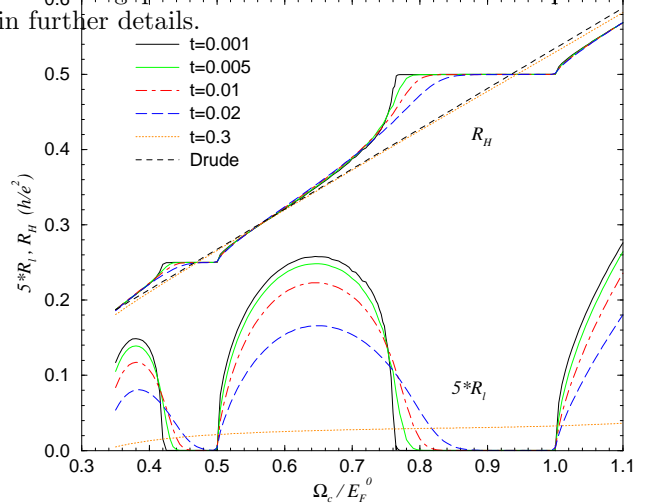


FIG. 8: Hall and longitudinal resistances versus magnetic field, calculated for different temperatures, $t = k_B T/E_F^0$. Sample parameters: $d = 1.5 \mu\text{m}$, $n_0 = 4 \cdot 10^{11} \text{cm}^{-2}$, $b = 0.952d$, $R = 10 \text{nm}$ and $\gamma_I = 0.1$, $\lambda = 30 \text{nm}$.

The temperature effect on the calculated resistance curves is shown in Fig. 8. As expected, the width of the QH plateaus increases monotonically with decreasing temperature, but apparently it has a finite limit for $T \rightarrow 0$. We have also included the high-temperature result for $k_B T/E_F^0 = 0.3$ (since $E_F^0 = 13.5 \text{meV}$, this means $T \approx 47 \text{K}$). At the low- B side of the figure $k_B T \sim \hbar\omega_c$, and the derivative of the Fermi function overlaps about two LLs. Since we consider only the lowest Landau levels ($n = 0, 1, 2$), our calculation is not correct in this limit. Nevertheless it is interesting to compare this result with the Drude result, which should be valid if the Shubnikov–de Haas oscillations are smeared out at higher the temperature.

In the Drude approximation we have $\rho_H(x) = \omega_c \tau_{tr} \rho_l(x)$, with $\rho_l(x) = 1/\sigma_0(x)$, where $\sigma_0(x) = e^2 \tau_{tr} n_{el}(x)/m$ is independent of the magnetic field. Inserting this into Eq. (17), we obtain

$$\frac{I}{E_y^0} = \frac{e^2 \tau_{tr}}{m} 2d \bar{n}_{el} = \frac{e^2}{h} \frac{2E_F}{\hbar/\tau_{tr}}. \quad (26)$$

In Eq. (18) we take the integrand to be $\omega_c \tau_{tr}$, but only for $|x| < b$, where $n_{el}(x)$ is not exponentially small, and obtain $V_H/E_y^0 = 2b \omega_c \tau_{tr}$. With Eq. (19) we obtain the

Drude result

$$R_H^D = \frac{h}{e^2} \frac{b}{2d} \frac{E_F^0}{E_F} \frac{\hbar\omega_c}{E_F^0}, \quad R_l^D = \frac{h}{e^2} \frac{\hbar/\tau_{tr}}{2E_F}. \quad (27)$$

The energies E_F and E_F^0 are calculated numerically from the density profile at $B = 0$, $T = 0$, as is described above, and τ_{tr} is calculated as described in the appendix, with $k_F = \sqrt{2\pi n_{e1}}$. The results are plotted as dashed straight lines in Fig. 8.

Finally, Fig. 9 shows the effect of the Landau level broadening on the QH plateaus at a fixed, relatively low temperature. The corresponding widths of the lowest LLs, in units of the cyclotron energy $\hbar\omega_c$, are given in Table II for the lowest and the largest B value shown in the figure. For the largest damping, the LLs start to overlap for $\hbar\omega_c/E_F^0 \lesssim 0.4$, so that the $\nu = 4$ QH plateau is not well developed. We note that the SCBA results summarized in the appendix are only valid at higher B values, where the LLs do not overlap.

The two high-mobility situation considered in Fig. 9 differ only by the range R of the Gaussian impurity potentials. The larger range leads to slightly smaller level broadening, but to much lower longitudinal resistance (i.e., to much higher mobility at $B = 0$).

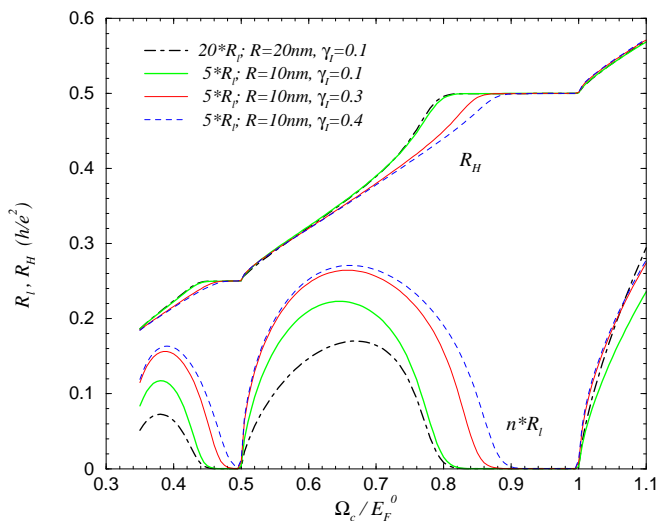


FIG. 9: Hall and longitudinal resistances versus magnetic field, calculated for different values of the collision broadening. Sample parameters: $d = 1.5 \mu\text{m}$, $n_0 = 4 \cdot 10^{11} \text{cm}^{-2}$, $b = 0.952d$, $\lambda = 30 \text{nm}$, $k_B T/E_F^0 = 0.01$ (i.e., $T = 1.57 \text{K}$).

C. Hall potential profile

The motivation of Ref. 5 and our present work came from the experimental investigation⁴ of the electrostatic potential distribution across a Hall bar under QH conditions, caused by an applied current. Ahlswede and coworkers^{4,7} observed three types of potential distribution, depending on the filling factor regime. Type I was

R	γ_I	γ_0^l	γ_1^l	γ_2^l	γ_0^h	γ_1^h	γ_2^h	$\mu_{B=0}$
20	0.1	0.117	0.085	0.073	0.043	0.037	0.033	747.5
10	0.1	0.161	0.123	0.105	0.071	0.051	0.044	75.1
10	0.3	0.482	0.369	0.316	0.213	0.152	0.131	8.34
10	0.4	0.643	0.492	0.421	0.284	0.203	0.175	4.69

TABLE II: Relative widths of the lowest Landau levels, $\gamma_n^l = \Gamma_n/\hbar\omega_c$ for $\hbar\omega_c/E_F^0 = 0.35$, and $\gamma_n^h = \Gamma_n/\hbar\omega_c$ for $\hbar\omega_c/E_F^0 = 1.10$, for the impurity parameters used in Fig. 9. First column: range in nm, last column: zero field mobility in m^2/Vs .

a more or less linear variation across the sample and is observed if the filling factor in the center is smaller and relatively close to (but not too close to) an integer n , i.e., $n \gtrsim \nu(0) \gtrsim n - 1/2$. If the center filling is slightly larger than an integer, $n < \nu(0) \lesssim n + 1/2$, type III is observed, characterized by a constant potential in the central region and a rapid variation across (narrow) strips, which move with decreasing B towards the sample edges and have been interpreted as incompressible strips.⁴ Finally, type II shows a rapid, non-linear variation of the potential in the center region and is observed if the center filling factor is very close to an integer.

In Ref. 5 it was shown that, in a local equilibrium picture, the changes of the electrostatic potential, caused by an applied current, follows closely the current-induced variation of the electro-chemical potential μ^* , so that the resulting density changes are small. In the present work we do not consider the feed-back of the spatial variation of μ^* on electrostatic potential and density profiles (linear response). But we expect from the results of Ref. 5, that, in the linear response regime, μ^* should show the same position dependence as the electrostatic potential would do, if the feed-back were calculated.

To calculate the Hall profile across the sample, we integrate $E_x(x)$, Eq. (16), from the center $x = 0$ to the actual x value. Typical results as functions of position x and magnetic field B are shown in Fig. 10. The normalization is chosen so that $V_H(B, x = d)/I = -V_H(B, x = -d)/I = R_H/2$. One sees clearly that the plateaus of the quantized Hall effect ($0.8 \lesssim \hbar\omega_c/E_F^0 \lesssim 1$ and $0.45 \lesssim \hbar\omega_c/E_F^0 \lesssim 0.5$) coincide with potential variation of type III, caused by current density confinement to the incompressible strips. Moving from a plateau region to smaller B values, the incompressible strips shrink and finally vanish, and the current density spreads more and more out into the bulk. This leads to the type I behavior ($0.52 \lesssim \hbar\omega_c/E_F^0 \lesssim 0.7$ and $\hbar\omega_c/E_F^0 \lesssim 0.4$). Immediately above the integer values of the center filling factor (in our approximation assuming spin degeneracy near $\nu(0) = 2$ and 4), we find the rapid variation of the type II. This is in very nice agreement with the experiment. Without our spatial averaging of the conductivity tensor, we would have missed the type I regions for $\hbar\omega_c/E_F^0 < 1$, as has been observed in Ref. 5.

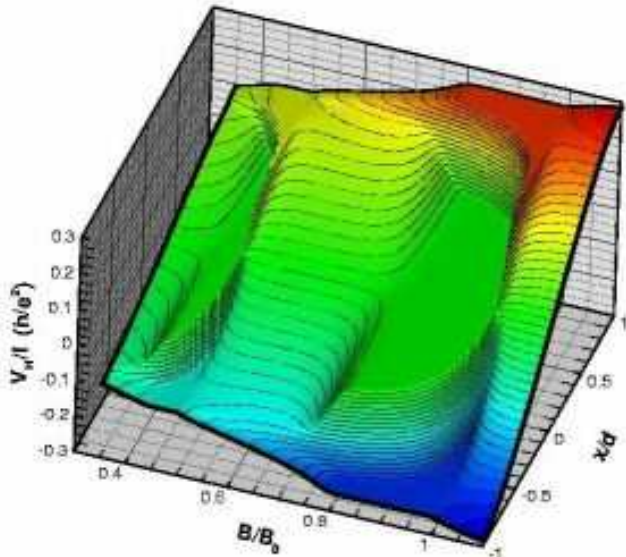


FIG. 10: Hall potential profile $V_H(x) = \int_0^x dx' E_x(x')$ across the sample, for varying $B/B_0 \equiv \hbar\omega_c/E_F^0$ and constant applied current I . Normalization: $[V_H(d) - V_H(-d)]/I = R_H$; sample parameters: $d = 1.5 \mu\text{m}$, $n_0 = 4 \cdot 10^{11} \text{cm}^{-2}$, $b = 0.952d$, $\lambda = 30 \text{nm}$, $k_B T/E_F^0 = 0.01$.

D. Summary

The virtue of our approach is, that it allows us to calculate resistance traces with exactly quantized quantum Hall plateaus of finite width, and with reasonable values of the resistances between these plateaus. While these intermediate resistance values depend on the details of our conductivity model, the quantized plateau values do not. The reason for this high accuracy and model-independence of the plateau values is the fact, that the latter are determined by the integrals in Eqs. (17) and (18) becoming singular across incompressible strips.

To obtain realistic widths of the QH plateaus, we had to consider a mechanism that prohibits singular current flow along very narrow incompressible strips. We have argued that small-scale non-local transport effects act into this direction, and that consideration of the finite extent of wavefunctions will prohibit arbitrarily narrow ISs at low magnetic fields, in contrast to the prediction of the Thomas-Fermi approximation. We were able to simulate such non-local effects by a simple spatial averaging procedure, with reasonable results for Hall and longitudinal resistance as functions of the magnetic field. Also the resulting potential profile, and therefore the current distribution across the sample, is in nice agreement with recent investigations.⁴ We consider this as a strong support for the relevance of our approach, notably because earlier approaches, which neglected dissipation, cannot explain the experiments, as has been discussed in Ref. 5.

Note that, for QH plateaus corresponding to filling fac-

tors $\nu \geq 4$, our results are qualitatively different from the conventional edge channel picture. The latter explains, for instance, the quantized conductance value $G = 4e^2/h$ as the sum of the contributions of two spin-degenerate, quasi-one-dimensional current channels near each of the opposite sample edges, thus tracing back the quantized Hall effect to the phenomenon of 1D conductance quantization (in a situation where no backscattering occurs).¹⁷ That is, the edge states, created by the LLs with quantum numbers $n = 0$ and $n = 1$, contribute both to the current in the plateau regime of the QHE. Our results, on the contrary, indicate that the total current flows along the incompressible strip with local filling factor $\nu(x) = 4$ (where both LLs $n = 0$ and $n = 1$ are occupied), whereas near local filling factor $\nu(x) = 2$ no incompressible strip and no contribution to the current exists.

Comparing our resistance curves with experiments, we notice that the high-field edge of a calculated plateau occurs at a magnetic field, at which an incompressible strip (with an even integer value of the effective filling factor $\nu_0 = 2E_F^0/\hbar\omega_c$) first occurs in the center of the sample. In experiments these ν_0 values usually are found somewhere near the centers of the plateaus. We have good arguments that this discrepancy is due to our neglect of long-range potential fluctuations due to the randomly distributed ionized donors. We have simulated the “short-range” part of the Coulomb potentials of the remote donors by Gaussian potentials, but we have neglected their overlapping long-range parts, which lead to long-range potential fluctuations. We have evaluated the short-range disorder within the SCBA to calculate conductivities and LL broadening. We have seen that with increasing disorder scattering the level broadening increases and, as a result, the widths of the QH plateaus shrinks. On the other hand, one knows from technical applications of the QH effect, that rather impure samples have usually especially wide and stable QH plateaus. This points to the role of long-range potential fluctuations, which become more important with increasing impurity concentration.

As a rough simulation of such long-range fluctuations, we have added oscillatory terms to the confinement potential and then repeated our calculations. We indeed find that such modulations can widen and stabilize the QH plateaus, and eventually even shift them to higher magnetic fields, depending on the amplitude, the range, and possible other details of the perturbation. This becomes understandable, if one considers the effect of such fluctuations on the existence and the position of incompressible strips. However, we do not want to discuss such considerations further, since we believe that our quasi-one-dimensional model is not appropriate for a reliable discussion of statistical fluctuations of a 2D donor distribution. Effects of long-range disorder in an unconfined 2D ES on the longitudinal resistance between QH plateaus have already been discussed a decade ago.¹⁸ This discussion seems however not applicable to the rather narrow samples of our present interest, since, first, the confinement affects the self-consistently calculated

potential and thus the density distribution,¹³ and, second, the early assumptions about current-carrying and isolating regions are not compatible with our results and the experimental findings.⁴

Acknowledgments

We gratefully acknowledge useful discussions with E. Ahlswede and J. Weis. This work was supported by the Deutsche Forschungsgemeinschaft, SP ‘‘Quanten-Hall-Systeme’’ GE306/4-2.

APPENDIX: SCBA CONDUCTIVITIES

The low-temperature, high-field magnetotransport, determined by elastic scattering of the 2D electrons by randomly distributed impurities with scattering potentials of arbitrary range, has been studied by Ando and coworkers.^{14,15,16} The results for the case of non-overlapping LLs can be summarized as

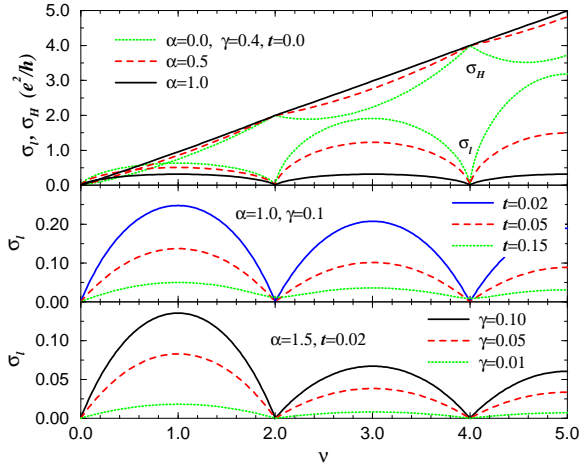


FIG. 11: SCBA results for longitudinal (σ_l) and Hall (σ_H) conductivity, in units of e^2/h , versus filling factor, at fixed magnetic field for different values of impurity range ($\alpha = R/l$) and strength ($\gamma = \Gamma/\hbar\omega_c$), and of temperature ($t = k_B T/\hbar\omega_c$). For the two lower panels the correction $-\Delta\sigma_H$ to $\sigma_H^0 = e^2\nu/h$ is negligible, and σ_H is not shown.

$$\nu = g_s \sum_{n=0}^{\infty} \int dE A_n(E) f(E - \mu), \quad (\text{A.1})$$

$$\sigma_l = g_s \sum_{n=0}^{\infty} \int dE \left[-\frac{\partial f}{\partial E} \right] \sigma_{xx}^{(n)}(E), \quad (\text{A.2})$$

$$\sigma_H = \frac{e^2}{h} \nu - \Delta\sigma_H, \quad (\text{A.3})$$

$$\Delta\sigma_H = g_s \sum_{n=0}^{\infty} \int dE \left[-\frac{\partial f}{\partial E} \right] \Delta\sigma_{yx}^{(n)}(E), \quad (\text{A.4})$$

with the spectral functions of widths Γ_n ,

$$A_n(E) = \frac{2}{\pi\Gamma_n} \sqrt{1 - \left(\frac{E - E_n}{\Gamma_n} \right)^2}, \quad (\text{A.5})$$

centered around the Landau energies (10), and

$$\sigma_{xx}^{(n)}(E) = \frac{e^2}{h} \frac{\pi}{2} \left[\Gamma_n^{xx} A_n(E) \right]^2, \quad (\text{A.6})$$

$$\Delta\sigma_{yx}^{(n)}(E) = \frac{e^2}{h} \frac{\pi^2}{4} \frac{\Gamma_n^{yx}}{\hbar\omega_c} \left[\Gamma_n^{yx} A_n(E) \right]^3. \quad (\text{A.7})$$

Assuming a single type of impurities with the Gaussian potential (23), these parameters can be expressed in terms of the integrals

$$(\Gamma_n^{(j)})^2 = \Gamma^2 \int_0^{\infty} dx g_n^{(j)}(x) \exp(-[1 + \alpha^2]x), \quad (\text{A.8})$$

where $\Gamma^2 = 4n_l V_0^2/(2\pi l^2)$ and $\alpha = R/l$, and the weight functions

$$g_n^{(0)}(x) = \left[L_n^0(\alpha^2 x) \right]^2, \quad g_n^{(d)}(x) = \frac{1-x}{2\alpha^2} g_n^{(0)}(x),$$

$$g_n^{(\pm)}(x) = \frac{x}{\sqrt{2n+1} \pm 1} L_n^0(\alpha^2 x) L_{n-(1\mp 1)/2}^1(\alpha^2 x)$$

are determined by the associated Laguerre polynomials $L_n^m(x)$. With these notations one obtains

$$\Gamma_n^2 = (\Gamma_n^{(0)})^2, \quad (\Gamma_n^{xx})^2 = (\Gamma_n^{(d)})^2, \quad (\text{A.9})$$

$$(\Gamma_n^{yx})^4 = (\Gamma_n^{(+)})^4 + (\Gamma_n^{(-)})^4. \quad (\text{A.10})$$

In the limit of short-range scattering potentials, $\alpha \rightarrow 0$, one has $\Gamma_n^2/\Gamma^2 = 1$, $(\Gamma_n^{xx}/\Gamma)^2 = n + 1/2$ and $(\Gamma_n^{yx}/\Gamma)^4 = n + 1/2$. With increasing α these parameters decrease and remain for $\alpha \gtrsim 1$ about an order of magnitude smaller than their $\alpha = 0$ values.^{14,15}

Some typical SCBA results are shown in Fig. 11. In general, σ_l and the correction $\Delta\sigma_H$ to the free electron Hall conductivity $\sigma_H^0 = e^2\nu/h$ decrease with increasing range of the scattering potentials.

At zero temperature, $\Delta\sigma_H$ is proportional to $\Gamma/\hbar\omega_c$ with a factor depending only on the range parameter $\alpha = R/l$. The longitudinal conductivity $\sigma_l(\nu)$, on the other hand, depends only on α and not on $\Gamma^2 =$

$(2/\pi)\hbar\omega_c\hbar/\tau_0$, i.e. depends not on the impurity concentration n_I and strength V_0 entering the $B = 0$ relaxation rate $\hbar/\tau_0 = n_I V_0^2 m/\hbar^2$. This is very different from the $B = 0$ conductivity $\sigma_0 = e^2 n_{el} \tau_{tr}/m$ obtained for the impurity model (23), which depends on $n_{el} = k_F^2/2\pi$ and via τ_{tr} on both the potential strength and range. For $B = 0$ collision broadening effects can be neglected, and one obtains for elastic scattering at the Fermi edge

$$\begin{aligned} \frac{\hbar}{\tau_{tr}} &= \frac{n_I m}{\hbar^2} \int_{-\pi}^{\pi} \frac{d\varphi}{2\pi} [v_q]_{q=k_F[2(1-\cos\varphi)]^{1/2}}^2 (1 - \cos\varphi) \\ &= \frac{\hbar}{\tau_0} [e^{-x}(I_0(x) - I_1(x))]_{x=(Rk_F)^2}, \end{aligned} \quad (\text{A.11})$$

where the last equality holds for our impurity potential

(23), with Fourier transform $v_q = V_0 \exp(-R^2 q^2/4)$, and $I_\nu(x)$ is a modified Bessel function. This leads for $Rk_F \gg 1$ to $\tau_0/\tau_{tr} \approx [\sqrt{8\pi}(Rk_F)^3]^{-1}$. With increasing temperature, the peak values of $\sigma_l(\nu)$ decrease and the minima at even integer ν values are no longer exponentially small for $k_B T/\hbar\omega_c \gtrsim 0.1$. This behavior of the SCBA results, shown in the middle panel of Fig. 11, is similar to that of the Gaussian model treated in Ref. 5. At finite temperature, the longitudinal conductivities $\sigma_l(\nu)$ increase with γ , i.e., with increasing scattering strength (bottom panel of Fig. 11). This is as expected from the Drude picture for $\omega_c \tau_{tr} \gg 1$: $\sigma_l \approx \sigma_0/(\omega_c \tau_{tr})^2 \propto 1/\tau_{tr}$.

-
- ¹ K. von Klitzing, G. Dorda, and M. Pepper, Phys. Rev. Lett. **45**, 494 (1980).
² H. Bachmair, E. O. Göbel, G. Hein, J. Melcher, B. Schumacher, J. Schurr, L. Schweitzer, and P. Warnecke, Physica E **20**, 14 (2003).
³ B. Kramer, S. Kettemann, and T. Ohtsuki, Physica E **20**, 172 (2003).
⁴ E. Ahlswede, P. Weitz, J. Weis, K. von Klitzing, and K. Eberl, Physica B **298**, 562 (2001).
⁵ K. Güven and R. R. Gerhardts, Phys. Rev. B **67**, 115327 (2003).
⁶ P. Weitz, E. Ahlswede, J. Weis, K. v. Klitzing, and K. Eberl, Physica E **6**, 247 (2000).
⁷ E. Ahlswede, J. Weis, K. von Klitzing, and K. Eberl, Physica E **12**, 165 (2002).
⁸ P. Weitz, E. Ahlswede, J. Weis, K. v. Klitzing, and K. Eberl, Appl. Surf. Sci. **157**, 349 (2000).
⁹ D. B. Chklovskii, B. I. Shklovskii, and L. I. Glazman, Phys. Rev. B **46**, 4026 (1992).
¹⁰ D. B. Chklovskii, K. A. Matveev, and B. I. Shklovskii, Phys. Rev. B **47**, 12605 (1993).
¹¹ K. Lier and R. R. Gerhardts, Phys. Rev. B **50**, 7757 (1994).
¹² J. H. Oh and R. R. Gerhardts, Phys. Rev. B **56**, 13519 (1997).
¹³ A. Siddiki and R. R. Gerhardts, Phys. Rev. B **68**, 125315 (2003).
¹⁴ T. Ando and Y. Uemura, J. Phys. Soc. Japan **36**, 959 (1974).
¹⁵ T. Ando, Y. Matsumoto, and Y. Uemura, J. Phys. Soc. Japan **39**, 279 (1975).
¹⁶ T. Ando, A. B. Fowler, and F. Stern, Rev. Mod. Phys. **54**, 437 (1982).
¹⁷ M. Büttiker, Phys. Rev. B **38**, 9375 (1988).
¹⁸ D. B. Chklovskii and P. A. Lee, Phys. Rev. B **48**, 18060 (1993).